The Effect of Open-to-Suburban Terrain Transition on Wind Pressures on a Low-Rise

Building

Sejin Kim¹, Nasrollah Alinejad², Sungmoon Jung³, and Ho-Kyung Kim⁴

Abstract

This study delves into the complex dynamics of upwind terrain transition from open country to suburban areas

and its effects on wind pressures and forces on low-rise buildings. Advanced wind tunnel experiments were

conducted, focusing on two critical distance parameters: the building's proximity to the upwind transition patch

and the patch's length. This approach allowed for a nuanced examination of the stochastic characteristics of

wind pressures, differing from standard open terrain scenarios. In addition, by comparing our results with con-

ventional open terrain exposures and aligning with ASCE 7-16 designated zones, this research offers novel in-

sights into the terrain transition impact on building design. These findings significantly advance our understand-

ing of wind load estimations in varied terrains, contributing valuable perspectives to structural design and wind

engineering.

Keywords: Low-rise building; Wind pressure; Upwind terrain transition; Wind tunnel test.

1. Introduction

The study of wind pressures on low-rise buildings, particularly in varied terrains, is a pivotal concern in

Assistant professor, School of Civil Engineering, Chungbuk National University, 1 Chungdae-ro, Seowon-gu, Cheongju, Chungbuk 28644, South Korea. Email: sejin0991@gmail.com

² Ph.D. candidate, Department of Civil and Environmental Engineering, FAMU-FSU College of Engineering, 2035 E Paul Dirac Dr, Tallahassee, Florida 32310, United States, Email: na19i@mv.fsu.edu

³ Professor, Department of Civil and Environmental Engineering, FAMU-FSU College of Engineering, 2035 E Paul Dirac Dr, Tallahassee, Florida 32310, United States. Email: sjung@eng.famu.fsu.edu (corresponding author)

⁴ POSCO Chair Professor, Department of Civil and Environmental Engineering, Professor, Institute of Construction and Environmental tal Engineering, Seoul National University, 1 Gwanak-ro, Gwanak-gu, Seoul 08826 South Korea. Email: hokyungk@snu.ac.kr

-1-

This file is the final accepted version of the manuscript published in https://doi.org/10.1016/j.jobe.2024.108651 wind engineering, crucial for designing structures resilient to extreme weather conditions. Over the past few decades, there have been numerous numerical and experimental studies to predict wind loads and pressure distributions on low-rise buildings in homogeneous terrain exposures [1–7]. These studies have helped to better understand and predict the mechanism of wind pressures and loads on low-rise buildings for homogeneous upwind terrain. Based on these previous studies most of current building design approach, such as ASCE 7-16 [8], provides pressure distributions over different archetype buildings assuming homogeneous upwind terrain for the safety and simplicity. However, the presence of surrounding buildings or changes in upwind terrain patch can interfere with wind flow, causing different pressure distribution results from those of an isolated low-rise building.

In recent decades, a number of research has focused on evaluating the wind pressure distribution on non-isolated buildings. Pioneering studies by Ho [9], Kiefer and Plate [10], and Holmes [11] have conducted wind tunnel experiments to measure the wind pressure distributions across groups of low-rise buildings, creating actual urban environments within wind tunnels. Based on the results, they pointed out the surrounding building condition can cause large variability in pressure fluctuation on building surfaces. Zhang and Li [12], along with Flaga et al. [13] and Chen et al. [14,15], who conducted wind tunnel tests with high-rise buildings within built-up areas, also reported that the configuration of surrounding buildings can cause significant distortions in wind angle and pressure on the surfaces of these buildings.

Further research has delved into the influence of the relative positioning of nearby high-rise buildings on wind pressure affecting target structures. A series of experiments [16–23] focused on two or three high-rise buildings. By varying their relative positions, these studies demonstrated that the proximity of neighboring buildings could significantly amplify pressure distributions due to vortex-shedding or channeling effect. Experiments focusing on low-rise buildings were also conducted by adjusting their relative spacing [24–27]. In a similar wind tunnel investigation, Ahmad and Kumar [28] noted considerable variations in wind pressure coefficients when examining the relative positioning of three low-rise buildings. Their results indicated a substantial

This file is the final accepted version of the manuscript published in https://doi.org/10.1016/j.jobe.2024.108651 increase of up to 73% in the minimum pressure coefficient and a decrease of up to 69% in the average pressure. Complementing these findings, Chen et al. [29] and Li et al. [30] conducted Computational Fluid Dynamics (CFD) simulations on clusters of low-rise buildings, involving three and nine buildings, respectively. These simulations highlighted a significant amplification of pressure, with observed increases reaching up to 70%. This points to the critical influence that the arrangement and orientation of buildings have on wind-induced pressure dynamics.

While extensive research has been conducted on wind pressure distributions influenced by surrounding buildings, a significant yet lesser-explored area in wind engineering is the impact of upwind terrain transitions. Studies by Tamura [5] and Wang and Stathopoulos [31] have emphasized the influence of upwind terrain within a range of 500 m to 1 km from buildings, underscoring the importance of considering broader terrain configurations in wind load assessments. However, most previous research has been focused on changes in wind profiles [32–36] with only a limited number of studies examining the effects of these terrain transitions on building pressure distributions. For example, the study by Wang and Stathopoulos [31], which aimed to assess the influence of wind conditions on building wind pressures, encountered limitations including restricted wind incident angles and a narrow range of terrain transition scenarios. This highlights the need for more experimental studies to fully understand the relationship between terrain changes and wind pressures on low-rise buildings.

This research gap is relevant considering the distinct wind flow dynamics induced by transitions from smooth (natural or less developed) to rough (urban or built-up) terrains, a common occurrence at the edges of urban expansion. These transitions can result in unique turbulence characteristics and altered wind patterns, thereby impacting the wind pressure exerted on structures. This study delves into the effects of proximity and length of upwind terrain transitions on the wind loads and pressures of low-rise buildings through wind tunnel testing. The focus is on the frequently observed transition from open country (z0 = 0.03 m) to suburban areas (z0 = 0.3 m) at suburban boundaries, as illustrated in Fig. 1. Despite the limited literature on building pressure response for such transitions, field measurements of wind from similar sites are available for reference [37].

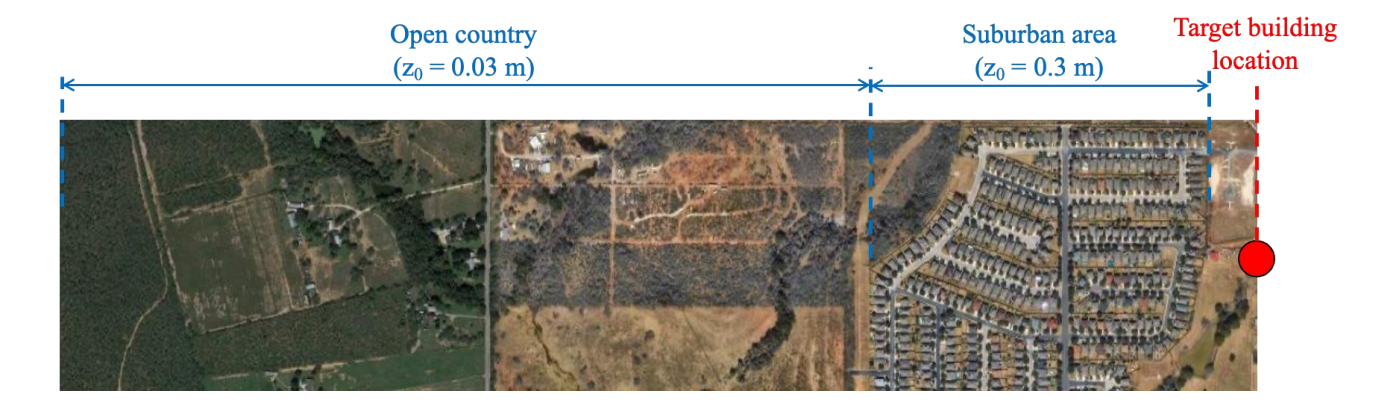


Fig. 1. An example of the interested building subject

In this study, two variables are experimentally controlled: the length of the upwind patch and its distance from the building, to simulate a variety of terrain transition scenarios. By comparing the pressure distributions to those on an isolated building in open terrain, this research aims to elucidate the effects of both proximity and length of the transition patch. Additionally, area-averaged pressure coefficients are computed in accordance with ASCE 7-16 [8], to assess their impact on building design. The study also explores the influence on overall body forces, including drag and lift, providing a comprehensive understanding of how upwind terrain transitions affect wind pressures and loads on low-rise buildings. These findings offer valuable insights for both theoretical and practical applications in structural design and urban planning.

2. Wind tunnel test

2.1 Wind tunnel facilities and building model

The wind tunnel experiments were conducted in the Boundary Layer Wind Tunnel (BLWT) at the University of Florida. The BLWT is equipped with 1,116 individually configurable roughness elements, arranged in a staggered pattern, to simulate the effects of terrain roughness on wind flow (see Fig. 2). Each roughness element has a plane dimension of 10 cm by 5 cm and its height can be adjusted to reflect changes in surface roughness. The aerodynamic roughness length (z_{θ}) was adjusted from 0.03 m to 0.3 m according to Eq. (1) to represent the transition from an open country to a suburban area. The smooth surface roughness of 0.03 m represents featureless

This file is the final accepted version of the manuscript published in https://doi.org/10.1016/j.jobe.2024.108651 areas, while the rough surface roughness of 0.3 m represents suburban terrain.

$$\frac{z_0}{H} = \left(1 - \frac{d_0}{H}\right) \exp\left[-\left\{0.5 \frac{C_D}{\kappa^2} \left(1 - \frac{d_0}{H}\right)^{-0.5}\right\}\right]$$
 (1)

where H is the height of the roughness element, C_D is the drag coefficient, d_0 is the zero-plane displacement, and κ is von Kármán's constant, which is equal to 0.4 [38].

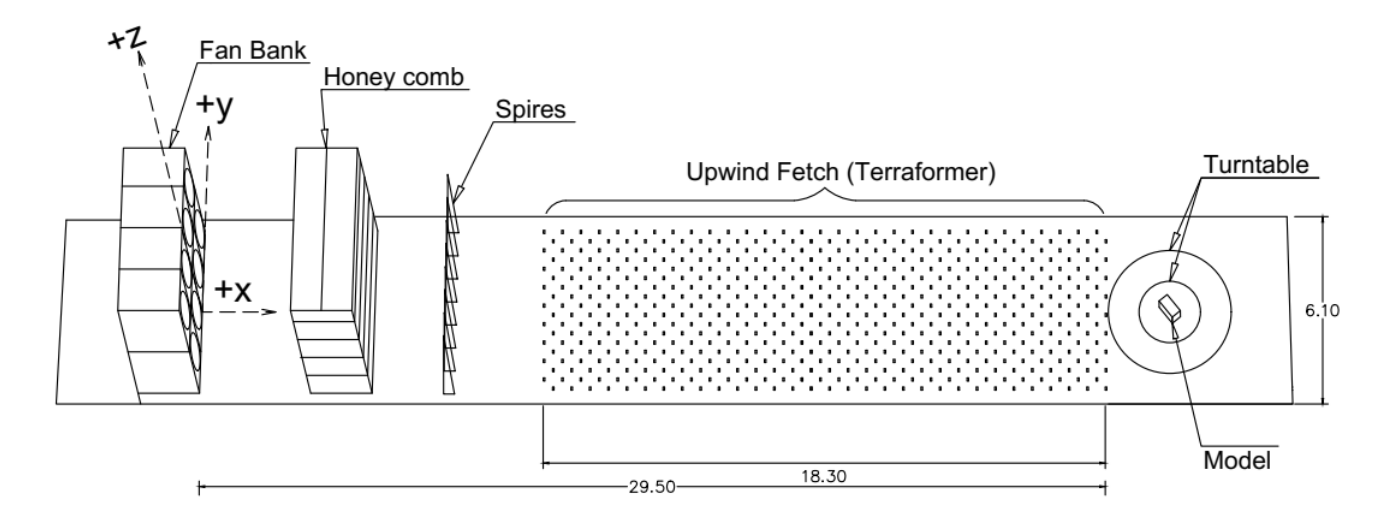


Fig. 2. Boundary Layer Wind Tunnel schematic plan view (dimensions in meters)

The wind speed was measured using three Cobra Probes located at (x=29.5 m, y=0.0) in the BLWT. The data was collected with a sampling rate of 1,250 Hz at 36 different heights, starting from 5 mm from the ground up to 1500 mm. The pressure distributions on the low-rise building model were measured using a 216 channel, 625 Hz Scanivalve ZOC33 pressure scanning system mounted under the turntable. Each pressure tab was linked to a corresponding channel using a tube measuring 1,345 mm in length with an inner diameter of 1.37 mm. To correct the distortion effects that arise as air flow passes through the tube, the measured pressure data was digitally filtered using the tubing system transfer function. The error of the pressure sensor is below \pm 3% for amplitude and less than approximately 6 degrees for phase.

The collected pressure data was filtered with a low-pass filter with a cutoff frequency of 200 Hz and recorded for 1 minute (corresponding to 10 minutes in full scale). The low-rise building model had dimensions of 8 cm (height) \times 18.25 cm (width) \times 27.45 cm (length) at a 1:50 scale and was equipped with a gable roof with a 2%

This file is the final accepted version of the manuscript published in https://doi.org/10.1016/j.jobe.2024.108651 slope. Fig. 3 illustrates the building model and the layout of the pressure taps on the surfaces. The blockage ratio was less than 3% across the entire experiments.

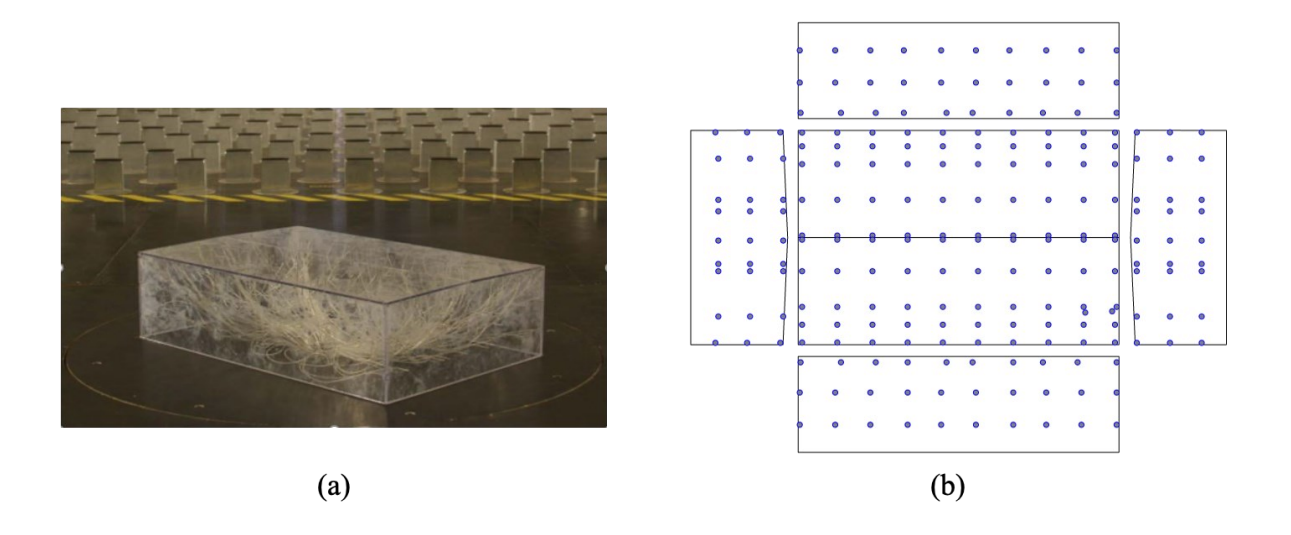


Fig. 3. Low-rise gable roof building model [7]

2.2 Test cases

Fig. 4 presents a schematic illustration of the test setup. It shows a suburban terrain patch placed in front of the low-rise building with the rest of the area as open terrain. The suburban patch length was varied by controlling parameters L and d. The parameter L represents the distance from the far end of the patch to the building. Based upon the findings presented by Wang and Stathopoulos [31], who suggested that the design load of a low-rise building is generally influenced by an upwind fetch length of 250 - 500 m, we selected five test points for our study, which are 189, 280, 372, 463, and 555 m in real scale. The parameter d represents the distance from the near end of the patch to the building, which has been conventionally set to about 2 m in the testing facility under homogeneous terrain conditions [7], equivalent to 100 m in real scale. In this study, we tested three different levels of d (25, 55, 100 m in real scale) to evaluate the impact of the distance between the patch and the building. To compare with conventional testing methods, one homogeneous terrain cases was also tested: open terrain.

This file is the final accepted version of the manuscript published in https://doi.org/10.1016/j.jobe.2024.108651
These comparisons aimed to better understand the effect of the size of the upwind transition patch and its distance from the building. Ten wind directions were tested from 0 to 90° with 10° intervals. The wind direction was manipulated by rotating the building model. This direction was then estimated by measuring the angle between the airflow in the tunnel and the roof ridge of the building model (see Fig. 4).

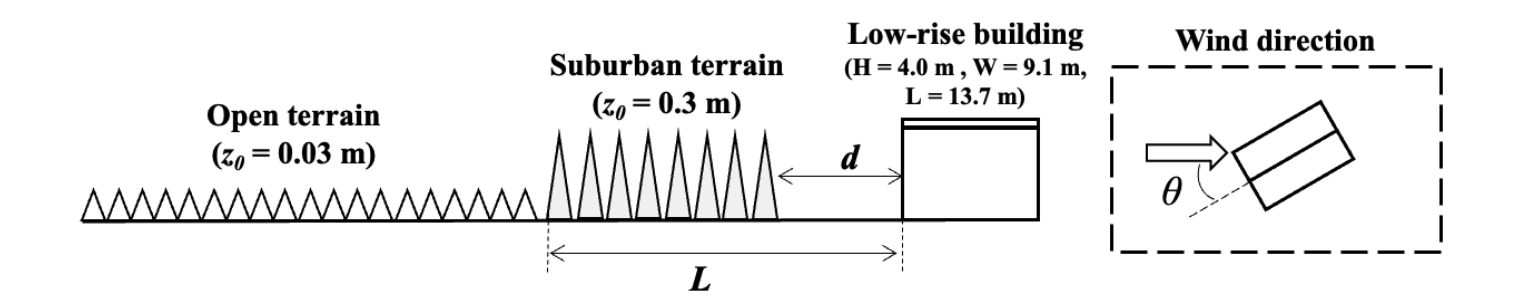


Fig. 4. Schematic illustration of the test setup

In order to demonstrate the impact of the transition terrains on the wind flow, this study analyzed variations in the mean wind speed and the turbulence intensity as illustrated in Fig. 5. These variations were examined over a vertical height range from 2.5 m to 15 m for distances of d = 25 and 55 m, and lengths of L = 189, 372, and 555 m. As a benchmark, profiles for open terrain are depicted as black dotted lines for comparative purposes. The ratio of mean wind speed at each measurement location to that at a 75 m height in the full-scale prototype is demonstrated in Fig. 5(a) and (b). Here, data for d = 100 m were omitted from Fig. 5 due to measurement errors, yet this exclusion does not undermine the overall findings of this study.

The analysis revealed several notable changes caused by the upwind transition terrain. First, there were discernible changes in the profile shapes along the height due to the upwind transition. In open terrain scenarios, both mean wind speed and turbulence intensity exhibit an exponential relationship with height, characterized by power-law exponents of 0.15 and -0.38, respectively. On the other hands, for transition terrains, the mean wind speed demonstrates a more linear relationship with height, and turbulence intensity remains relatively constant below 8 m, indicative of the influence of the upwind transition.

Second, the mean wind speed was reduced when a transition patch was placed before the building, implying the possibility of shielding wind flow and mitigating the overall wind speed at the building location. For example, Fig. 6(a) demonstrates the variations of the mean wind speed at 5 m height. According to the figure, the mean wind speed decreased more than 8% and 15% when *d* was 55 m and 25 m, respectively. Additionally, the mean wind speed decreased as *d* decreased and *L* increased, suggesting that the reduction in wind speed becomes greater as the patch gets closer to the building and its length increases.

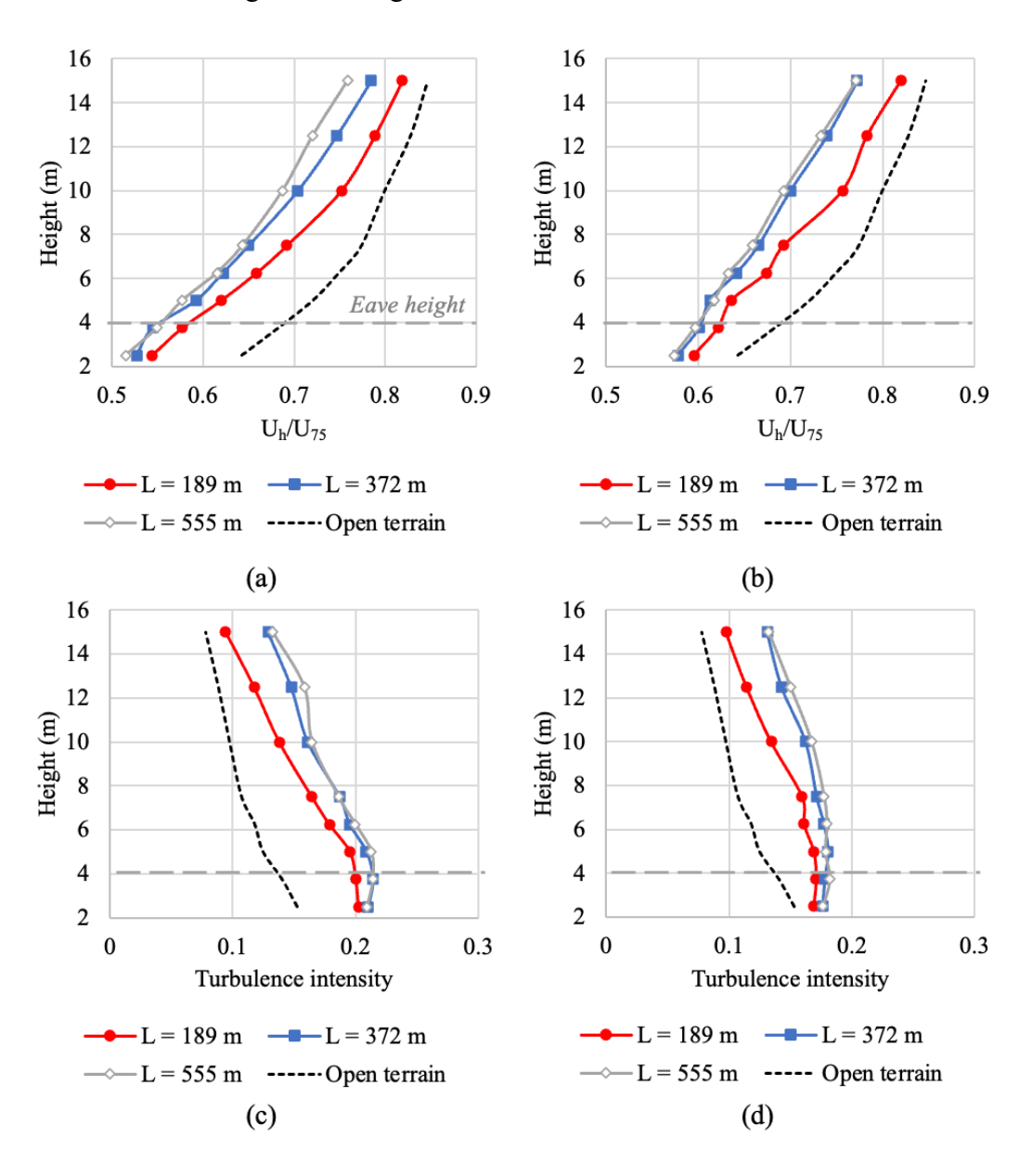


Fig. 5. Vertical profiles (2.5 - 15 m) of the ratio of mean wind speed for (a) d = 25 m and (b) d = 55 m, and the

turbulence intensity for (c) d = 25 m and (d) d = 55 m

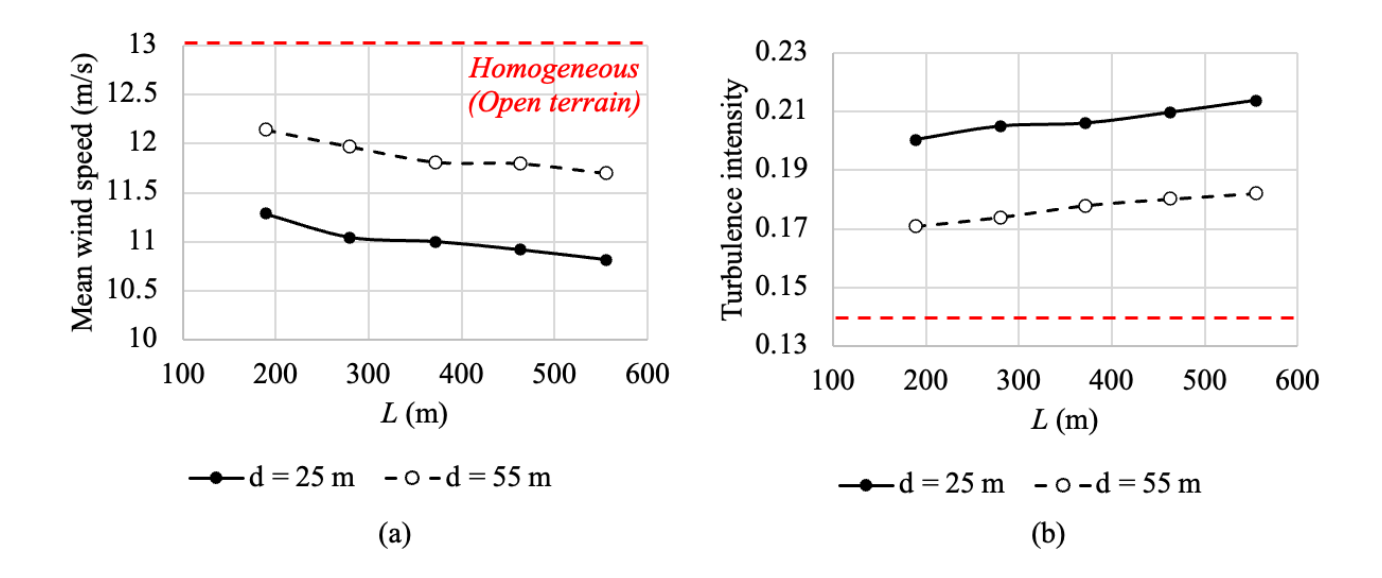


Fig. 6. Variation of wind properties at 5 m height (a) mean wind speed, (b) turbulence intensity

On the other hand, the turbulence intensity showed the opposite tendency with much larger intensities than in the homogeneous open terrain as shown in Fig. 6(b) due to the disturbance of the upwind transition patch. Fig. 7 demonstrates an example of power spectral density of the wind at 5 m height when L was 280 m. This figure clearly shows that the open terrain scenario presents a lower spectral density across the entire frequency range compared to the transition cases. Moreover, the transition case with d = 25 m demonstrates higher spectral densities than the case with d = 55 m. These disparities indicate that the upwind transition terrain can amplify all turbulent components, regardless of a decrease in the mean wind speed.

In addition, it was observed that wind properties above the 6-8 m range showed minimal variation with changes in *d*. In contrast, wind properties below this range were significantly influenced by this parameter. This differential effect underscores the critical influence of proximity to the upwind transition patch, particularly impacting wind properties at the eave height of low-rise buildings. Conversely, wind properties at higher elevations appeared to be more sensitive to variations in the length of the transition patch.

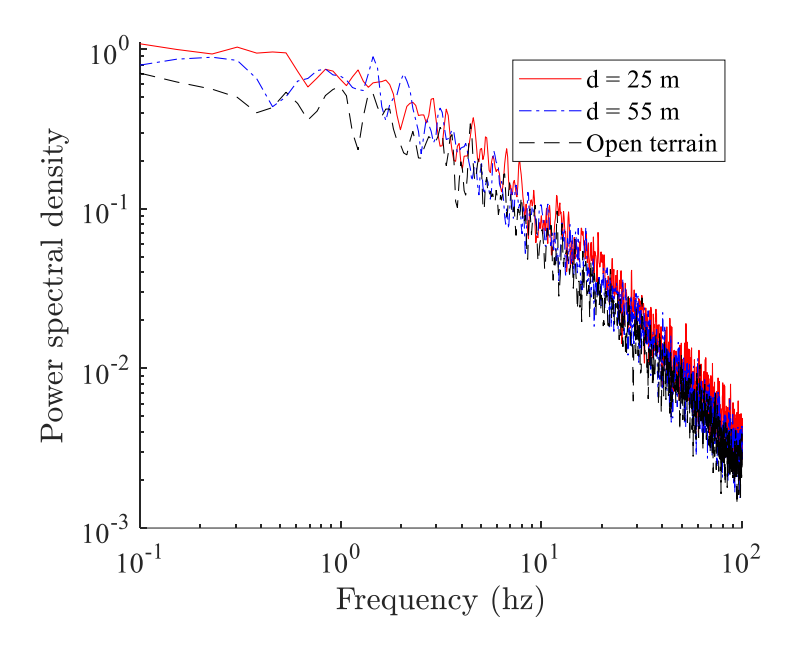


Fig. 7. Power spectral density of the wind at 5 m height (L = 280 m)

3. Pressure distributions on the building surfaces

The distributions of pressure coefficients over the building surfaces were observed while changing the two parameters, d and L, and the wind direction. For concise presentation, two representative groups of pressure taps were presented, shown as Sections A and B in Fig. 8. Section A, which is marked by blue line with white circles, is the cross-section along the ridge, which is 3.0 m away from the ridge in the real scale. Section B, which is marked by red line with red squares, is the centerline perpendicular to the ridge. Pressure coefficient C_p was estimated based on Eq. (2), where P_k is the pressure at k-th pressure tap, P_{static} is the static pressure, U is the reference wind speed (13 m/s), which is the mean wind speed at the eave height under the homogenous open terrain. For the purpose of evaluating changes in pressure magnitude, a consistent wind speed was applied across all transition cases. ρ is the air density (1.225 kg/m³).

$$C_p = \frac{P_k - P_{static}}{0.5\rho U^2} \tag{2}$$

This file is the final accepted version of the manuscript published in https://doi.org/10.1016/j.jobe.2024.108651

The pressure coefficient changes for the two sections were analyzed for three wind directions, representatively: 0° , 40° , and 90° . To enhance clarity, we represented the results of the homogeneous open terrain case and five transition cases, selected based on the parameters d and L: 1) d = 25 m & L = 189 m, 2) d = 55 m & L = 189 m, 3) d = 100 m & L = 189 m, 4) d = 100 m & L = 372 m, 5) d = 100 m & L = 555 m.

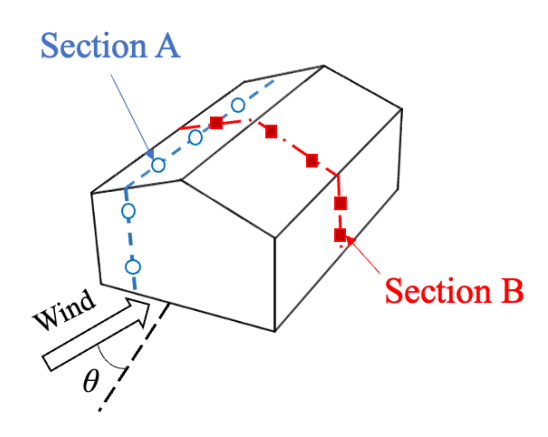


Fig. 8. Representative pressure tap groups: sections A and B

Figs. 8, 9, and 10 illustrate the distributions of mean, root-mean-square (RMS), and peak pressure coefficients along sections A and B, respectively, for the selected wind directions and transition cases. The peak pressure coefficient was determined using the Cook-Mayne method [39] assuming the extreme distribution of the wind pressure follows Fisher-Tippett type I as follow:

$$C_p^{peak} = U_p + 1.4/a_p \tag{3}$$

where U_p is the mode and a_p is the dispersion. Each set of pressure data's time history was segmented into six sub-samples, and six peak pressure coefficients were extracted from each subdivision. Using the Best Linear Unbiased Estimators (BLUE) method [40], we calculated the mode and dispersion presented in Eq. (3) based on these six peak pressure coefficients. As a result, a representative peak value which corresponds to non-exceedance probability of 78%.

The results of the five transition cases are depicted with solid or dotted lines, while the homogeneous open terrain case serves as a reference and is represented by bright blue points. The results showed a consistent trend

This file is the final accepted version of the manuscript published in https://doi.org/10.1016/j.jobe.2024.108651 in the pressure coefficient distributions, aligning with findings from previous research [1,27]. Observing the windward surface of the roof, when the wind direction was 0 or 90° , a large vortex resulted in high negative mean and peak pressure coefficients and high RMS values. At a wind direction of 40° , two significant corner vortices were observed on both windward edges of the roof, contributing to the observed bumps in the pressure coefficients of section A. However, the main focus of this study is the effect of the distance parameters, d and d, on the pressure coefficient distributions. The notable differences in the pressure coefficient variations with respect to d and d will be discussed in detail.

3.1 Mean pressure coefficients

The mean pressure coefficient results, shown in Fig. 9, revealed that the open terrain case had the highest values among all pressure taps compared to the transition cases. The mean coefficient decreased by 10-60% based on the parameters d and L. For instance, at the windward corner of section A, the magnitude of the coefficient decreased from -2.46 to -2.14 (13% decrease) as L increased from 189 m to 555 m, with d and wind direction being 100 m and 40° respectively. This shows that longer upwind suburban patches lead to lower mean wind pressures on the building surfaces. However, the decreasing rate of mean wind pressure slowed down significantly when L was large enough. These results are in line with previous studies [31], which showed that a roughness patch farther than 250 to 500 meters from the building does not significantly affect the wind loads on the building. The parameter d had a greater impact compared to d. For example, at the same pressure tap, the mean wind coefficient decreased significantly from -2.43 to -1.44 (42% decrease) when d decreased from 100 m to 25 m and d was kept at 189 m. This indicates that a closer transition region has a much stronger impact on reducing the mean wind pressure on low-rise buildings as well as the mean wind speed.

The findings show that the presence of an upwind suburban transition zone consistently decreases the mean pressures on the building's surfaces. The impact is greater as the length of the transition patch increases and the distance from the building decreases. This trend aligns with the results in Fig. 5, which highlight that the mean

This file is the final accepted version of the manuscript published in https://doi.org/10.1016/j.jobe.2024.108651 wind speed at the eaves height plays a key role in determining the distribution of mean pressure on the building's surfaces.

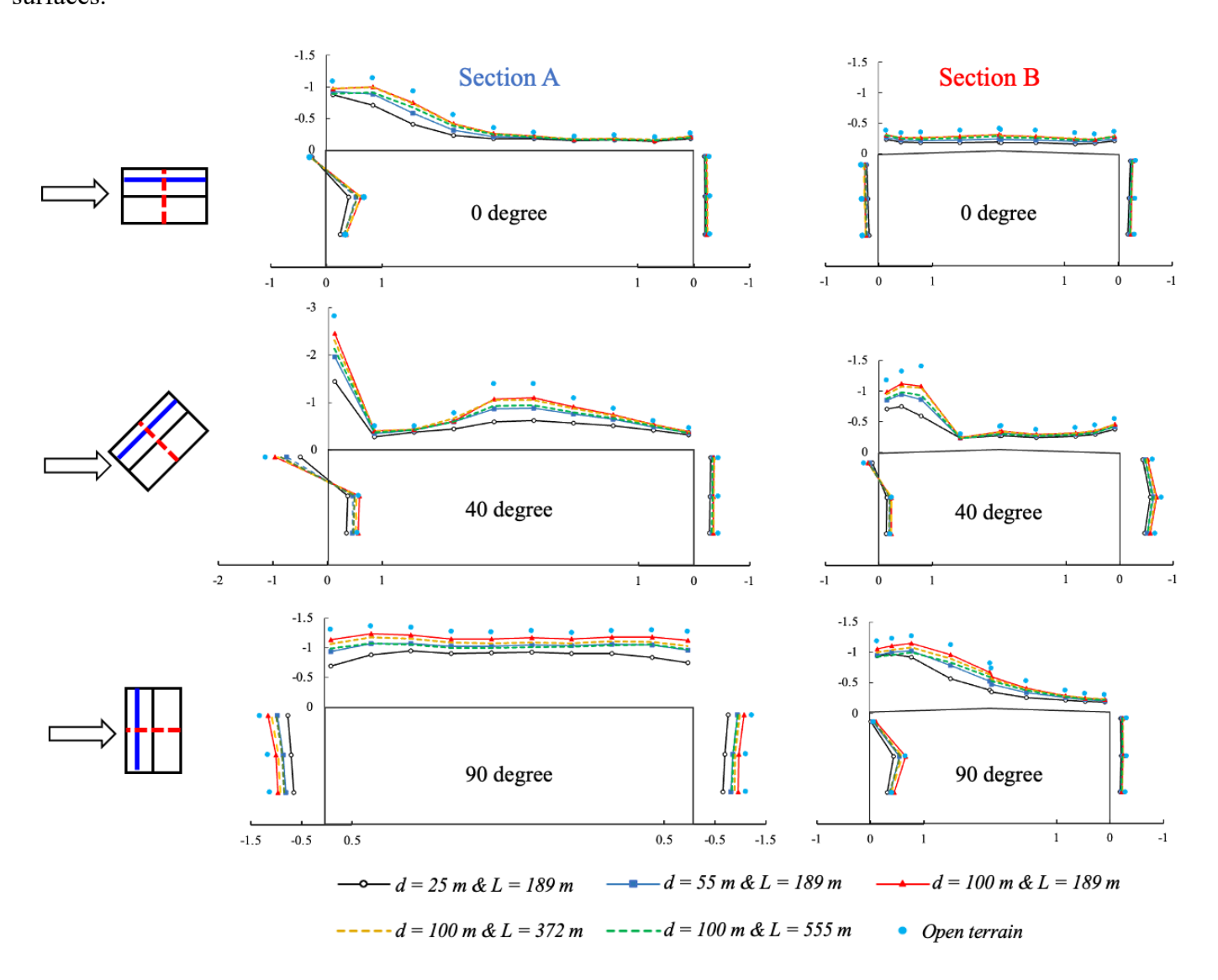


Fig. 9. Distributions of the mean pressure coefficients along sections A and B

3.2 Root-mean-square (RMS)

The results indicated that the RMS values were impacted by the presence of an upwind transition patch and wind direction. As shown in Fig. 10, when the wind direction was 0°, the RMS values were higher in the open terrain compared to the transition cases. However, when the wind direction was 40° or 90°, some of the transition

This file is the final accepted version of the manuscript published in https://doi.org/10.1016/j.jobe.2024.108651 cases had larger RMS values than the open terrain. For example, with a wind direction of 40° and a distance of *d* = 100 m, the RMS values at the windward corner of section A roof ranged from 0.54 to 0.62, whereas the open terrain case had an RMS value of 0.56. The disturbance effect of the upwind transition patch resulted in higher turbulence intensities as shown in Fig. 5, which caused large fluctuations in wind pressures on the building surfaces, despite the lower mean wind speed and pressure.

The results also occasionally showed that the RMS of pressure coefficient increased at the windward corners as the transition patch became closer to the building, as indicated by a decrease in the parameter d, when the wind direction was 0° or 90° . At the windward corner of the roof of section A, for example, the RMS value was 0.32 when d = 25 m and 0.30 when d = 55 m with wind direction of 0° , compared to 0.26 for the open terrain. Similar results were found for the windward roof corner of section B when the wind direction was 90° . The RMS values ranged from 0.36 to 0.40 for d = 25 m and 0.32 to 0.39 for d = 55 m, while they were 0.30 to 0.33 for the open terrain. Additionally, for section A when the wind direction was 90° , most of the pressure taps on the roof showed maximum RMS values when d was 25 m, while the open terrain case had minimum values. This trend was opposite to what was observed on other pressure taps, which showed a decrease in RMS values as d decreased due to the reduction in mean wind speed. These results indicate that even though the overall mean wind speed may decrease when the building is closer to the transition patch, the fluctuations in wind pressures can increase due to the disturbance effect, particularly at the windward surface of the building roof.

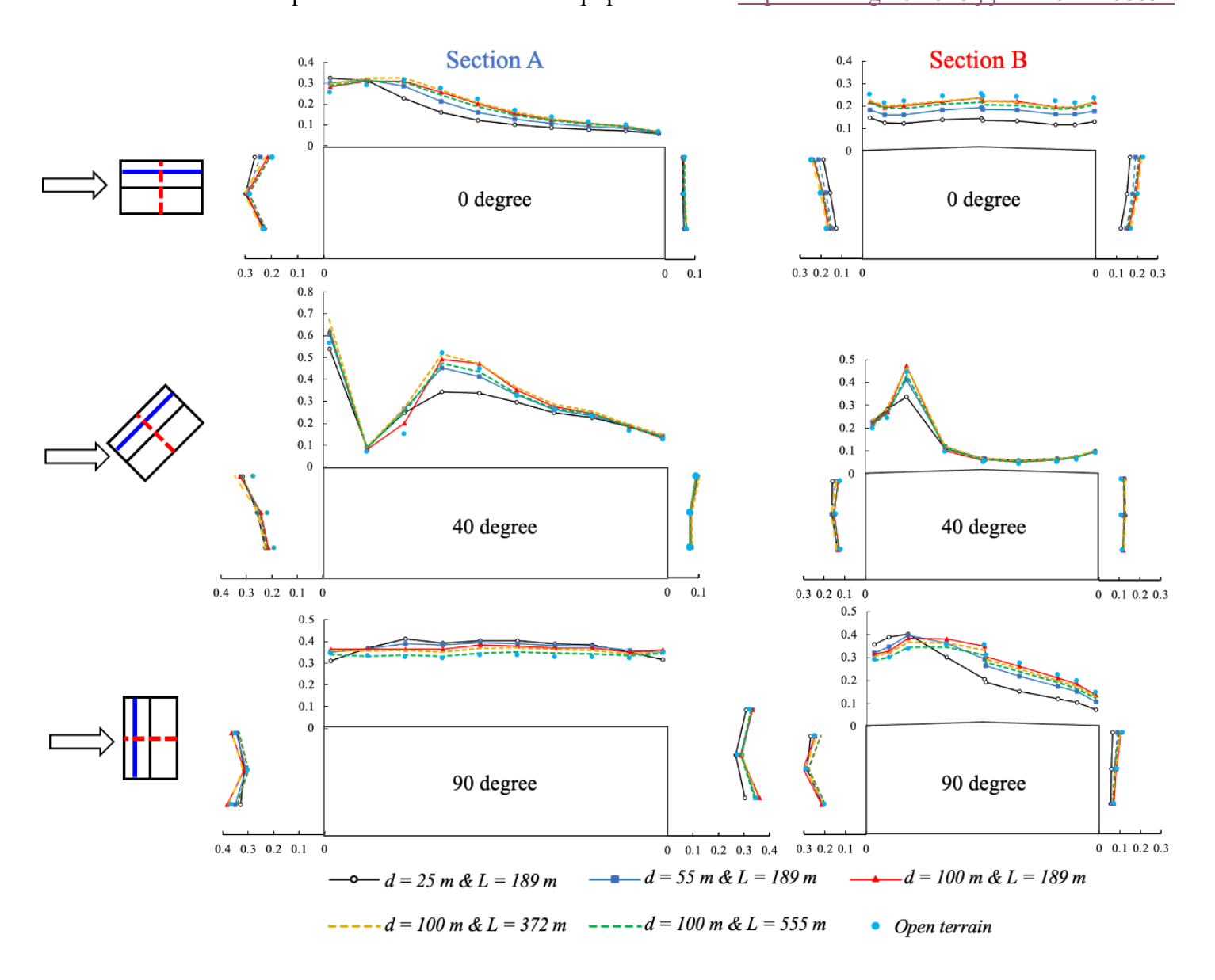


Fig. 10. Distributions of RMS of the pressure coefficients along sections A and B

3.3 Peak pressure coefficients

The distributions of the peak pressure coefficients on building surfaces are shown in Fig. 11. Unlike the mean pressure coefficients, the peak pressure coefficients in the transition cases were comparable to those in the open terrain case due to the significant fluctuations in wind pressure, as discussed in the previous section. The effect of parameter L was not significant; the average peak coefficient across all pressure taps changed by less than 4% from 189 m to 555 m. Also, there was only a 10% decrease in the peak coefficient when d decreased to This file is the final accepted version of the manuscript published in https://doi.org/10.1016/j.jobe.2024.108651
25 m, which was much smaller than the change in mean coefficients. Some pressure taps even showed increased peak coefficients with the upwind transition compared to the open terrain case. For example, a 9% increase in the peak coefficient was observed at the windward roof corner of section B when d and the wind direction were 25 m and 90°, respectively.

Fig. 12 displays the variation of the average peak pressure coefficients for three pressure taps located at the windward corner of section B for 40° and 90° wind directions, as indicated by the orange circle with the red dotted boundary in Fig. 11. The dotted black line represents the results from the open terrain scenario. As seen in Fig. 12, when the wind direction was 40° , the homogeneous terrain case had the highest peak pressure coefficients. On the other hand, when the wind direction was 90° , the transition cases had comparable or even higher coefficients than the homogeneous terrain case. This demonstrates that the presence of an upwind transition can either reduce or increase the peak wind pressure on building surfaces, depending on the upwind transition conditions and relative wind direction. There was no clear relationship between the peak coefficients and parameter L due to the interplay between changes in mean wind speed and turbulence intensity.

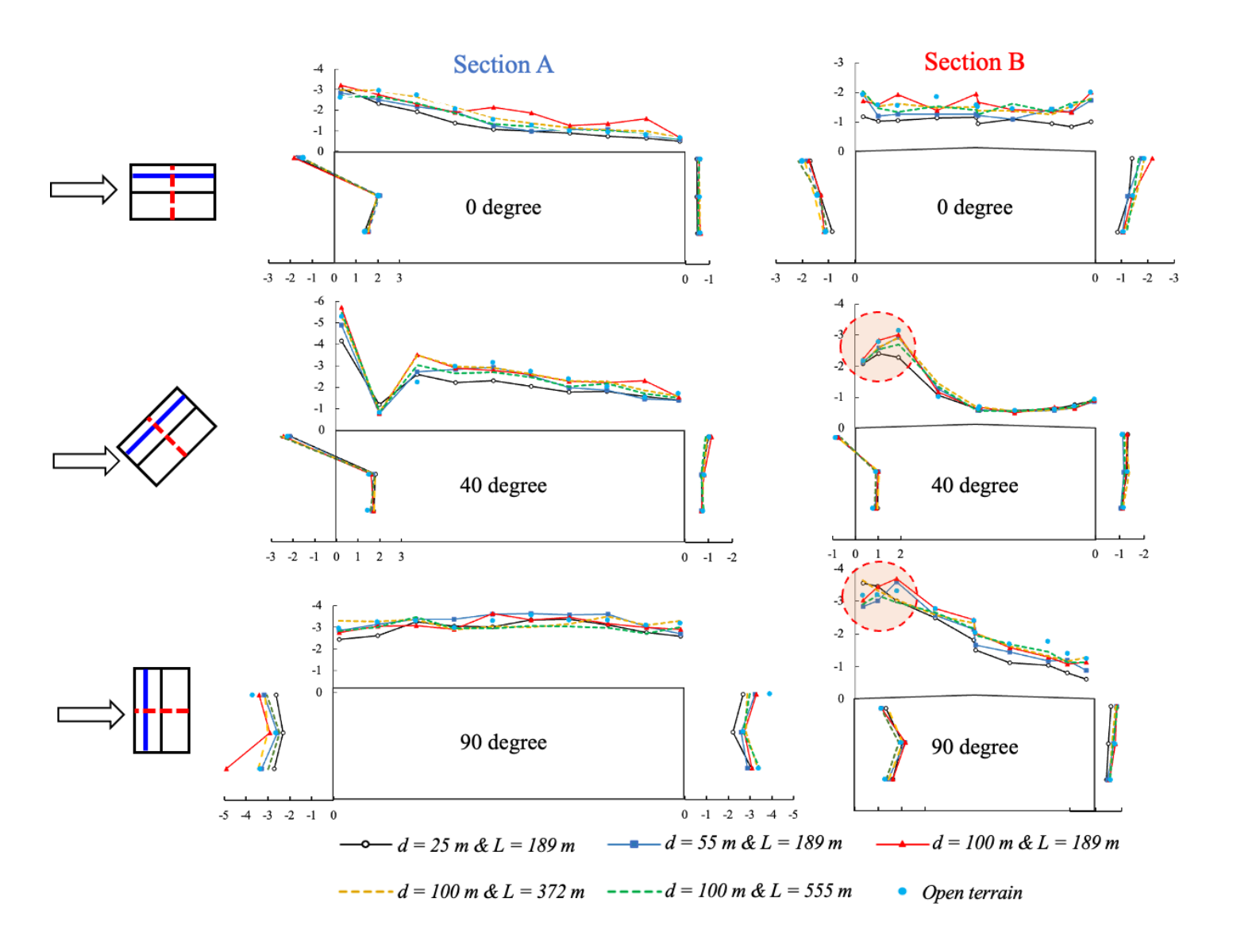


Fig. 11. Distributions of peak pressure coefficients along sections A and B

This file is the final accepted version of the manuscript published in https://doi.org/10.1016/j.jobe.2024.108651

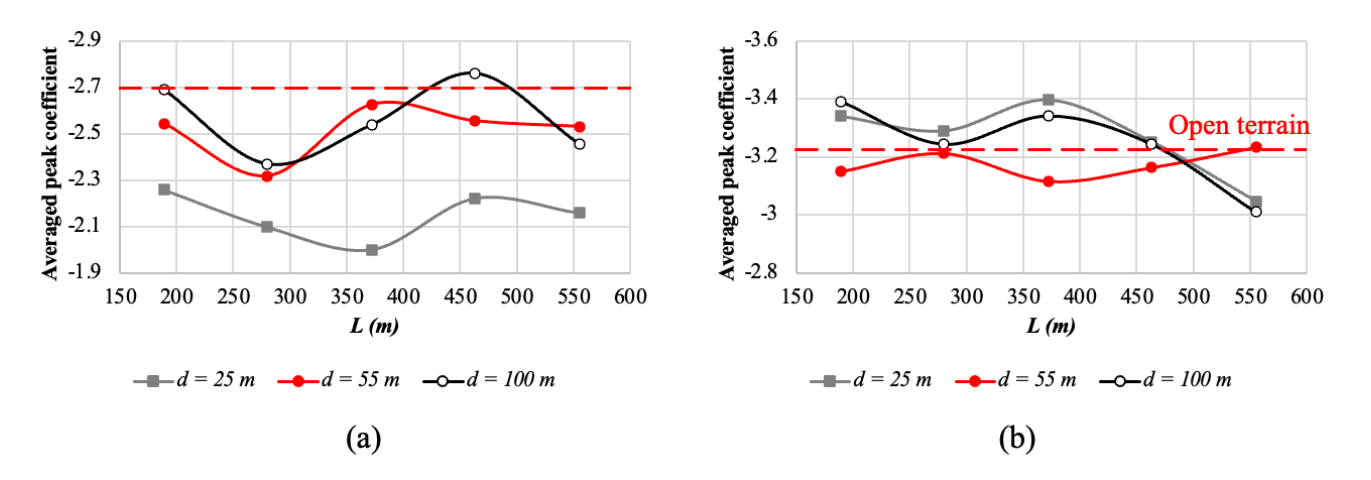


Fig. 12. Averaged peak coefficients on windward surface of section B for wind direction (a) 40° and (b) 90°

3.4 Skewness and kurtosis

To analyze the impact of the upwind transition on the statistical characteristics of wind pressures, we calculated the skewness and kurtosis, which are the measures of the asymmetry and skewness of a probability distribution. Skewness indicates the presence of negative or positive outliers, and a lower skewness means a distribution that contains values much less than the mean. Kurtosis measures the frequency of outliers and a kurtosis greater than 3.0 indicates a distribution with more outliers than a normal distribution.

Fig. 13 demonstrates the variations of the calculated skewness and kurtosis according to the parameters d and L for three example pressure taps. The two pressure taps at the windward corner and edge on the roof were chosen, which experienced substantial negative wind pressures when the wind direction was 40° and 90° , respectively. The last tap near the center of the front surface experienced a large positive pressure when the wind direction was 0° . The dotted lines indicate the skewness and kurtosis obtained from the homogeneous open terrain case for each wind direction.

The results revealed two clear trends. Firstly, in most cases, the absolute values of skewness and kurtosis for the transition cases were higher than those for the open terrain case. This indicates that the upwind transition patch results in a greater frequency and magnitude of negative peak pressures for Cases 1 and 2, and positive peak

This file is the final accepted version of the manuscript published in https://doi.org/10.1016/j.jobe.2024.108651 pressures for Case 3, compared to the open terrain case if the mean and RMS of wind pressure are equal. These increased statistical parameters are a key factor contributing to the high peak pressure coefficients in Figs. 10 and 11.

Secondly, the absolute value of skewness and kurtosis increased as the parameter *d* decreased, indicating that as buildings get closer, the frequency of outliers increases. However, the impact of parameter *L* was negligible, emphasizing that terrain patch far from the target building have limited influence. When assessing the wind pressure on a specific building, it's crucial to consider the location of the nearest building, which can reduce the mean wind speed but also result in frequent outliers in wind pressures.

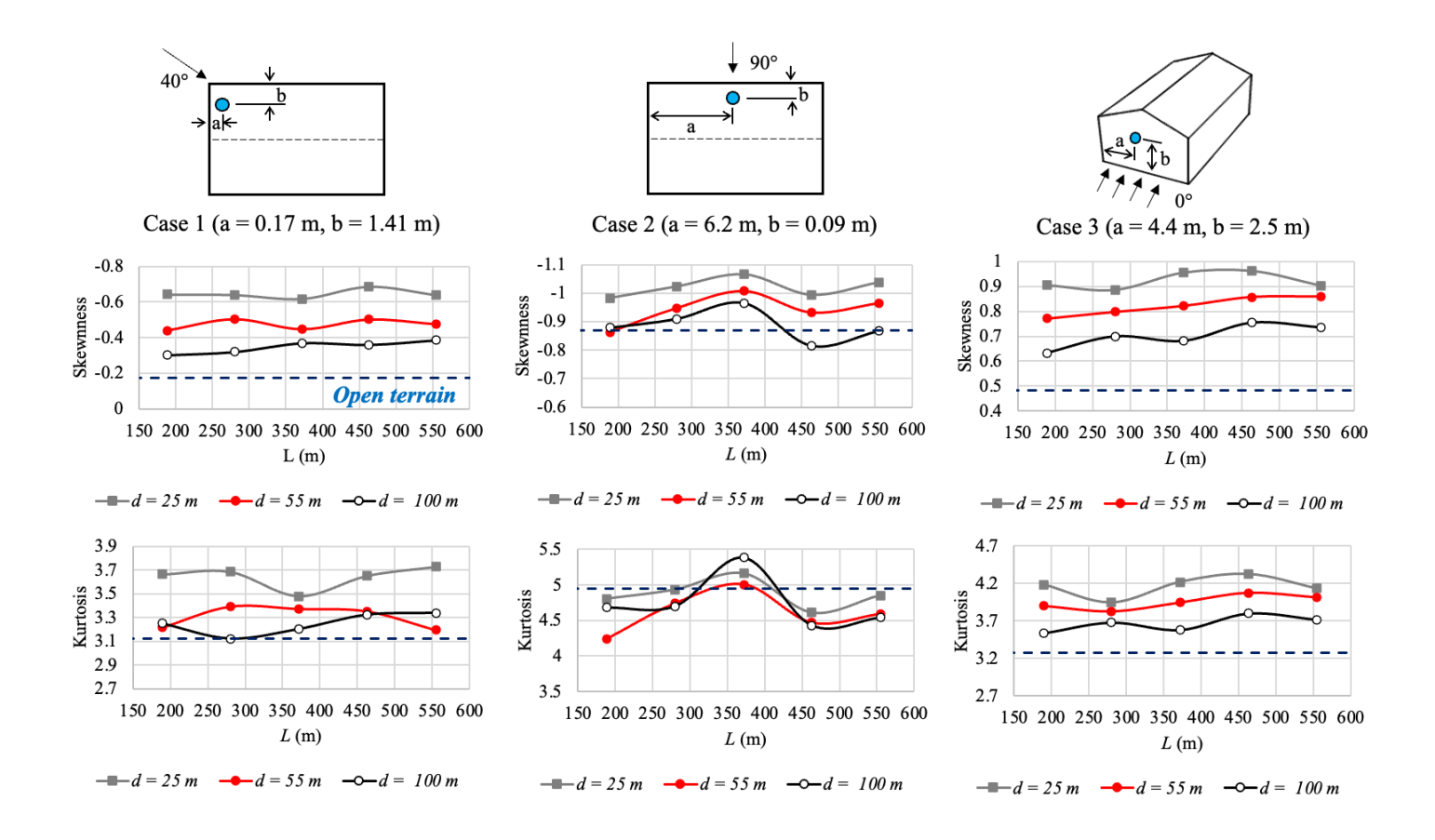


Fig. 13. Variations of skewness and kurtosis at three different pressure taps according to d and L

4. Area-averaged pressure coefficients

4.1 Wind loads on designated zones

Area-averaged pressure coefficients were obtained based on the zoning principle introduced by ASCE 7-16 [8] to evaluate the influence of the upwind transition patch on the overall surface of the building. Fig. 14 shows the 18 zones designated based on ASCE 7-16, and ten of them were selected, which were considered essential for the design application. The time histories of area-averaged pressure were obtained with consideration of the tributary area of each zone. The maximum and minimum instantaneous wind pressure coefficients experienced by each zone were selected among the entire time histories obtained from all wind directions. Table 1 shows the maximum positive and minimum negative pressure coefficients and related wind directions from the homogeneous open terrain case.

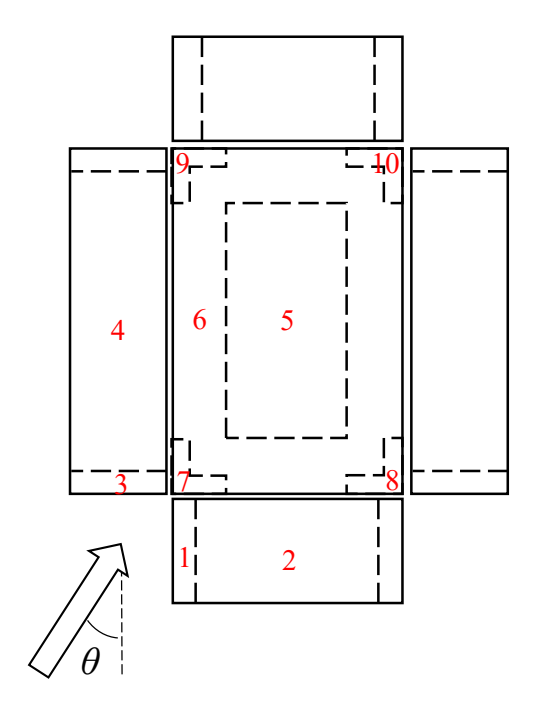


Fig. 14. Zone designation based on ASCE 7-16

Table 1. Maximum and minimum coefficient and direction of each zone of the open terrain case

Surface	Zone	Maximum		Minimum	
		Pressure coefficient	Wind direction	Pressure coefficient	Wind direction
Windward	1	1.64	40°	-2.54	80°

This file is the final accepted version of the manuscript published in https://doi.org/10.1016/j.jobe.2024.108651

wall	2	1.12	0°	-1.14	90°
	3	1.66	40°	-2.33	10°
	4	1.01	80°	-0.79	0°
Roof	5	-0.05	0°	-1.46	80°
	6	-0.11	0°	-1.19	40°
	7	-0.10	60°	-3.88	50°
	8	0.08	90°	-2.65	0°
	9	0.04	0°	-2.93	90°
	10	0.18	90°	-1.36	70°

The ratios of the maximum and minimum pressure coefficients between the homogeneous open terrain and the transition cases were calculated for the distance parameter d and L. As the tendency of the ratios for the parameter L was not clear, the ratios were averaged for all five Ls (189 – 555 m). Fig. 15 demonstrates the variations of the averaged ratios of the maximum and minimum pressure coefficients of the ten zones according to parameter d. Ratios that exceeds 1.0 indicates an amplification of pressure compared to the open terrain case. In the case of maximum coefficient, only the ratios of the windward front (zones 1 and 2) and side walls (zones 3 and 4) were presented because positive pressures on the roof were negligible with respect to the design application, as shown in Table 1. Fig. 16 depicts the rates of change in pressure coefficient according to d based on the linear least square regression method to evaluate the tendency of the ratio in the range of 25-100 m. This figure pertains exclusively to those zones where an amplification of the pressure coefficient (ratio > 1.0) is observed.

According to Fig. 15(a), the ratios of the maximum positive pressure coefficients of the front and side walls always exceeded 1.0. This indicates the maximum positive pressure coefficients of the front and side walls increased due to the presence of open-to-suburban transition. The amplification of pressure increased from 1.05 to 1.13 (5-13% increment) as the distance between the suburban patch and the building (d) increased. Fig. 16(a) also indicates an increase of approximately 0.07–0.09% for each unit meter of d, with the exception of zone 1. This represents a ratio increment of 7-9% for 100-meter change in d. It is essential to take into account this amplified

This file is the final accepted version of the manuscript published in https://doi.org/10.1016/j.jobe.2024.108651 positive pressure when calculating design wind loads for claddings or wall components accurately. Please note that these trends we found were based on the data up to d = 100 m. The tendencies might vary for greater distances.

Fig. 15(b) illustrates the ratios of the minimum pressure coefficient. When *d* was 25 m, it is noted that the majority of the zones had ratios beneath 1.0. This suggests a mitigation of negative pressures in comparison to the open terrain scenario, attributable to the drop in average wind speed. Most zones revealed an escalating trend in the ratio relative to *d*, which can be ascribed to the increments in mean wind speed. For instance, zones 1 and 3 - the windward edge of the side walls - exhibited pressure coefficients comparable to those in open terrain scenarios when *d* was 25 m, with ratios approximating 1.0. However, as *d* increased, the ratios for zones 1 and 3 escalated, reaching up to 1.11, indicating a 11% increase when *d* was 100 meters. In addition, zones 7, located on the windward corners of the roof, experienced a more rapid increase as *d* changed. The ratio here surged dramatically from around 0.82 to 1.06, a significant increment of 24%. These tendencies also can be observed in Fig. 16(b).

Considering the ratios of zones 1, 3, and 7, it becomes evident that the windward corners of the roof, along with the windward edge of the walls, may undergo more than a 10% increase in negative wind pressures in relation to the upwind transition. These results suggest that some of the edges or corners of the surfaces are particularly sensitive to turbulence intensity, which could cause significant wind pressure fluctuations. This might result in larger peak suction pressures than those found in uniform open terrain. On the contrary, the ratios of zones 2, 4, 5, and 6 remained persistently far below 1.0, implying reduced negative pressures compared to those experienced in the open terrain scenario. This suggest the large zones located in the center of each surface are more reliant on the average wind speed rather than the turbulent intensity.

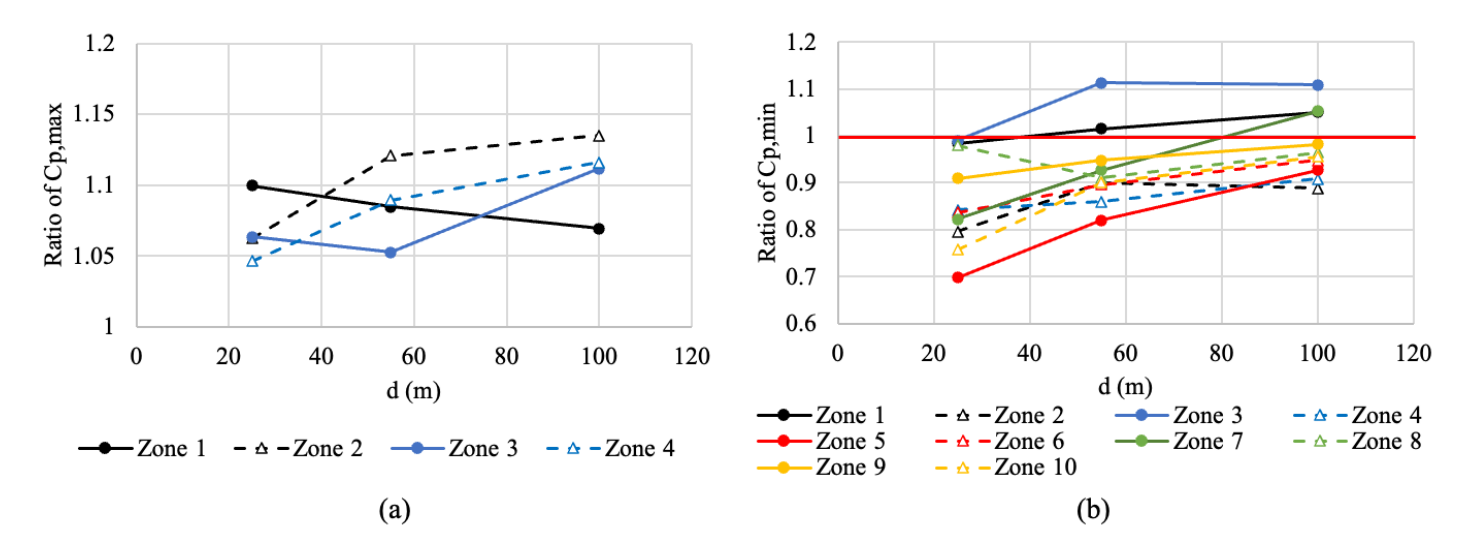


Fig. 15. Ratio of wind loading between the homogeneous open terrain and open-to-suburban transition (>1 means increase due to transition): (a) maximum and (b) minimum pressure coefficient

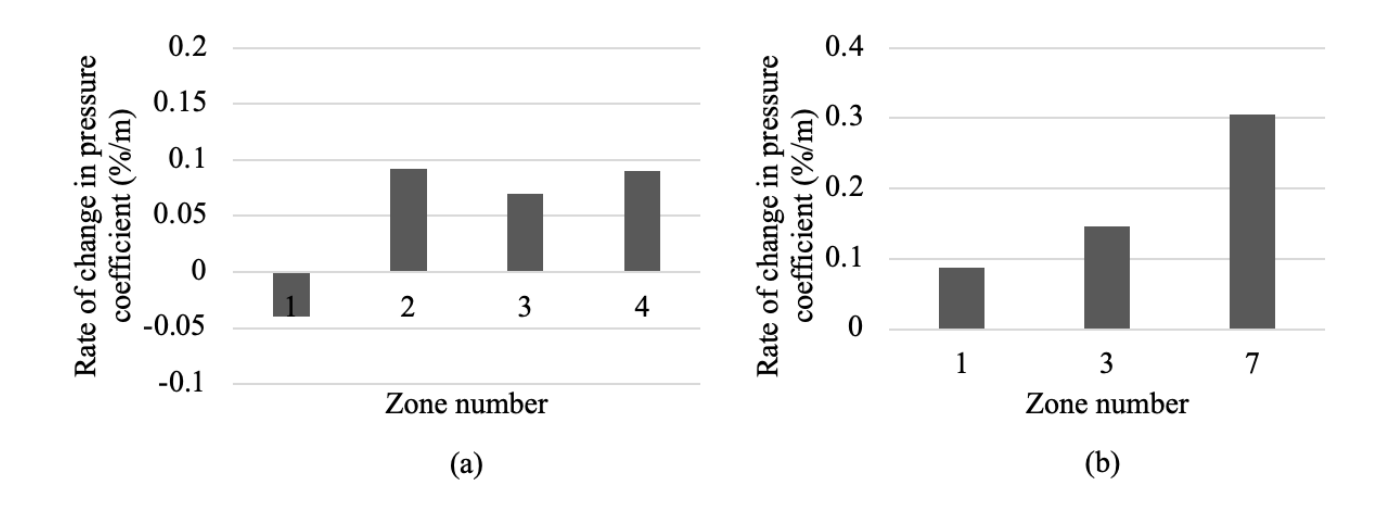


Fig. 16. Change in wind loading due to increasing d in open-to-suburban transition for the zones that had amplification: (a) maximum (zones 1, 2, 3, and 4) and (b) minimum pressure coefficient (zones 1, 3, 7, and 10)

Supplemental analysis was performed, specifically focusing on zone 7 due to its significant relevance to design objectives. Fig. 17(a) illustrates the variation in the ratio of minimum coefficients in relation to d for this zone. The black line maps the average ratio across all five L values, and the two red lines represent the scope of one standard deviation from this average. Grey circles are used to indicate individual measurements for each L

This file is the final accepted version of the manuscript published in https://doi.org/10.1016/j.jobe.2024.108651 value. As demonstrated in Fig. 17(a), the averaged ratio has a clear increasing tendency according to d, total 24% increment in the ratio as the d shift from 25 m to 100 m. Also, the ratio displays variability among different L values, reaching a zenith of 1.10 when d is set at 100 m. This suggests that the presence of the upwind transition can potentially result in an increment exceeding 10% in the peak pressure on zone 7.

Fig. 17(b) depicts the change in ratio relative to L. It can be inferred from Fig. 17(b) that there exists a slight upward trend in the ratio with respect to L for all three d cases. The average rate of change in the pressure coefficient was around 0.003% per unit meter of L, which is over hundred times smaller than the change rate associated with d. There was an approximate 2% increase in the pressure when L transitions from 189 m to 555 m. In contrast, a steeper 24% increment was observed when d elevates from 25 m to 100 m. Drawing from these results, it can be concluded that the presence of the upwind transition could serve as a critical factor during the design process, even when the length of the transition patch is relatively short.

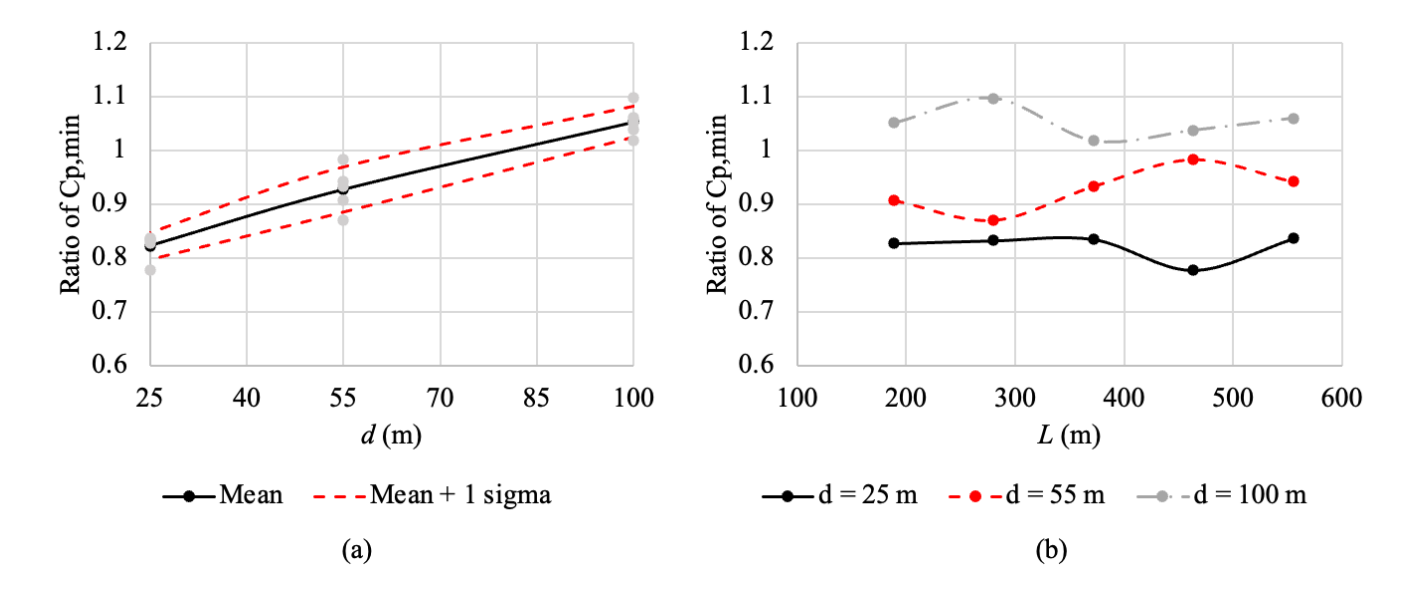


Fig. 17. Variation of the ratios of the minimum pressure coefficient of zone 7 according to (a) d and (b) L

4.2 Total drag and lift forces

Time histories of total body forces, drag and lift forces, were calculated by integrating all wind pressure data considering the tributary area of each pressure tap. The mean and peak forces were determined based on the

This file is the final accepted version of the manuscript published in https://doi.org/10.1016/j.jobe.2024.108651 integrated results, and the corresponding aerodynamic coefficients were calculated using Eq. (4).

$$C_{i,mean} = \frac{F_{i,mean}}{1/2\rho U^2 A} \qquad C_{i,peak} = \frac{F_{i,peak}}{1/2\rho U^2 A} \qquad (i = D \text{ or } L)$$

$$\tag{4}$$

where $C_{i,mean}$ and $C_{i,peak}$ are the mean and peak aerodynamic coefficients, and subscript i indicates drag (D) and lift (L) forces. $F_{i,mean}$ and $F_{i,peak}$ are the mean and peak wind forces. ρ is the air density $(=1.225 \text{ kg/m}^3)$, and U is the reference wind speed (=13 m/s), and A is the frontal area. The coefficients were obtained for each wind direction. Fig. 18 shows the variation of the mean and peak of drag and lift coefficients according to the wind direction. The mean and peak drag coefficients had maximum values of 1.30 and 1.98, respectively, at the 50° wind direction. Those lift coefficients were maximum at 80°, and the values were -0.78 and -1.22, respectively.

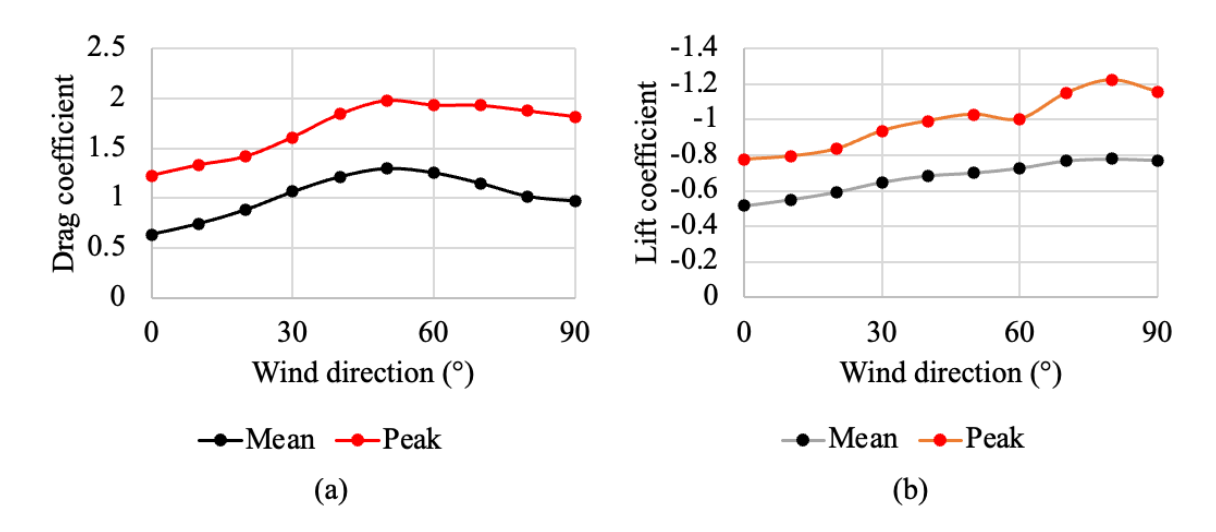


Fig. 18. (a) Drag and (b) lift force coefficients of the open terrain

The ratios of the transition cases to the open terrain case for the mean and peak coefficients were estimated. The ratio was obtained at 50° wind direction for the drag coefficient and 80° for the lift coefficient, which are the wind directions with the highest values for the drag and lift coefficients, respectively. The impact of parameters d and L on these ratios was also analyzed.

Fig. 19 and Fig. 20 show the estimated variations of ratio for the mean and the peak coefficients, respectively. All the ratios of the mean force coefficients depicted in Fig. 19 were lower than 1.0 due to the reductions in the mean wind speed. The data showed small declines in the ratios according to the distance parameter L, and

This file is the final accepted version of the manuscript published in https://doi.org/10.1016/j.jobe.2024.108651 a significant decrease in relation to the parameter *d*, due to the decreasing mean wind speed.

According to Fig. 20, the majority of the peak coefficient ratios were less than 1.0, yet they were larger than those presented in Fig. 19 due to the large fluctuation in the wind loads. When d was 100 m, the ratios of the drag force were found to be either similar to or slightly greater than 1.0 attributed to the large positive pressures present in zones 1, 2, 3, and 4. Then, the ratio dropped significantly as d decreased to 25 m. In the case of the lift force, all the ratios of the peak coefficients were lower than 1.0 even when d = 100 m. Despite the large suction pressures at the windward corner of the roof, zones 5 and 6, which have a much larger area than zone 7, predominantly determined the lift force. From these findings, we can infer that although the upwind transition might augment local pressure, it primarily serves to mitigate the overall forces acting on the building.

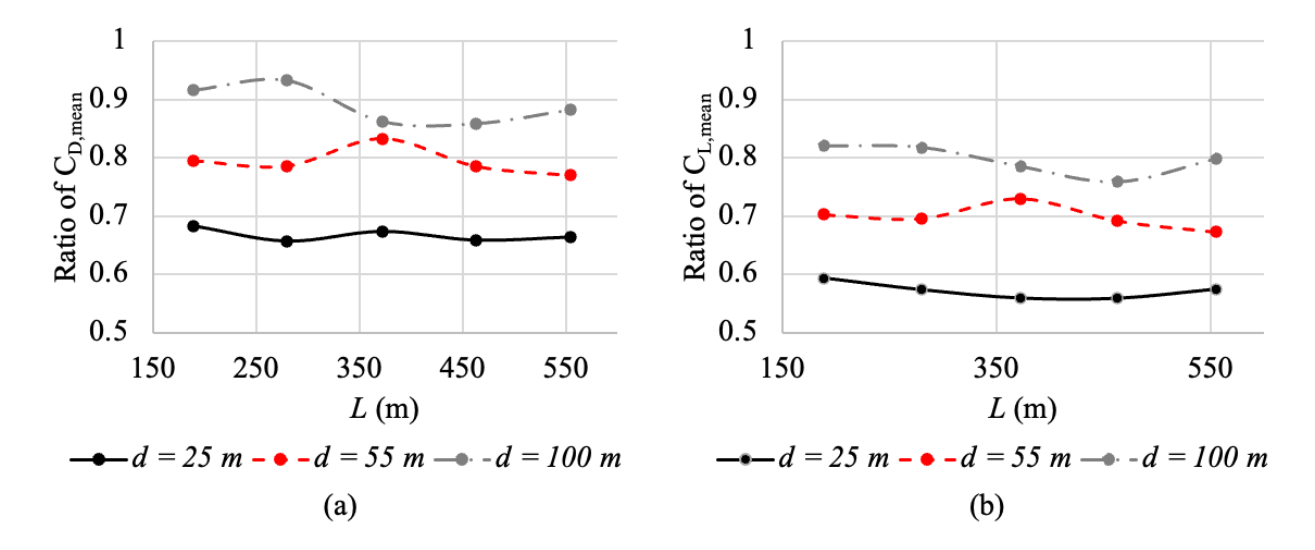


Fig. 19. The ratios of the mean coefficients. (a) drag and (b) lift forces

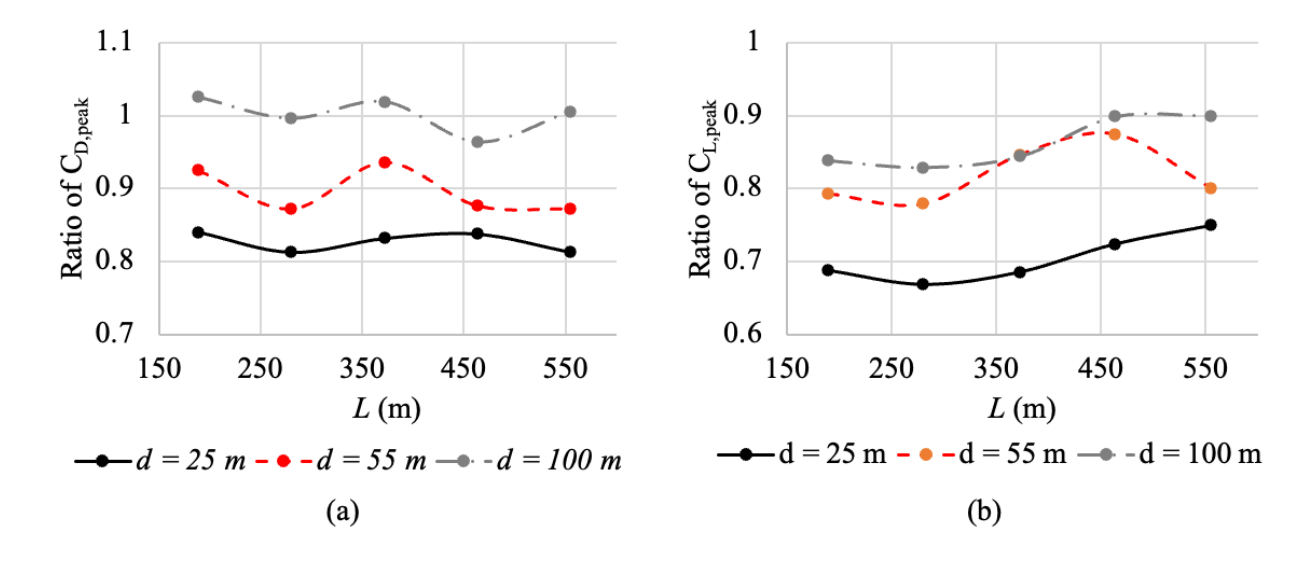


Fig. 20. The ratios of the peak coefficients. (a) drag and (b) lift forces

This study contributes to the understanding of upwind terrain transitions from open to suburban areas on wind pressures for low-rise buildings. However, it is important to note the limitations in our approach. The building model specifications and the range of terrain transition scenarios we have explored, while varied, do not cover all possible conditions. Real-world terrain transitions are complex and diverse, and our scenarios represent just a selection of these possibilities. Consequently, more comprehensive studies are needed to further explore this area. Despite these limitations, the outcomes of our research provide valuable insights into the effects of considering upwind terrain transitions, offering a foundational understanding for future explorations in this field.

5. Conclusions

This study aimed to evaluate the effect of the upwind open-to-suburban transition terrain patch on the pressure distributions of a low-rise building. We observed variations of pressure distributions on the building surfaces through wind tunnel tests. The distance between the building and the terrain patch as well as the size of the terrain patch were varied (distance from the building to the near end: 25 - 100 m, far end: 189 - 555 m).

This file is the final accepted version of the manuscript published in https://doi.org/10.1016/j.jobe.2024.108651
The conclusions of the experiments were as follows:

- (1) The upwind transition patch consistently reduced the mean wind speeds at the location of the investigated building, resulting in decrements in the mean pressure distributions on the building surfaces. The total integrated drag and lift body forces of the building decreased up to 30% due to the reduced mean wind speed. This mitigation effect on the wind pressures increased as the building moved closer to the transition patch, or the patch length increased.
- (2) The upwind transition patch caused an increase in the turbulence intensity of the wind, leading to an increase in the fluctuation component of wind pressures. Despite the decrease in mean pressures, the RMS and peak pressure coefficients can be similar to or even higher than those obtained in the homogeneous open terrain case especially on the windward corners.
- (3) According to the area-averaged calculations, the upwind transition intensified the peak positive and negative pressures exerted on the windward edges and corners of the building up to 11% (d = 100 m case). The negative peak suction pressure on the windward corner experienced up to 10% increment. The distance between the near end of the upwind transition patch and the investigated building was the most influential factor for peak pressure coefficients.
- (4) The skewness and kurtosis of the probability distribution of the pressure were also changed due to the influence of the upwind transition that their absolute values were greater than those of the open terrain. This tendency indicates that the upwind transition area can induce much more frequent and larger peak pressures if the mean and RMS of wind pressure are identical.
- (5) According to the experiment results, intensifications of local peak pressures could occur, especially on windward edges or corners of buildings depending on the relative location of the buildings to the upwind transition patch. Therefore, even if the length of the upwind transition patch is not long, it is recommended to consider the possibility of amplification.

Acknowledgment

This material is based upon work supported by the National Science Foundation under [Grant No. CMMI-1856205] and Basic Science Research Program through the National Research Foundation of Korea funded by the Ministry of Education [Grant No. 2022R1A6A3A03065716]. Any opinions, findings, and conclusions or recommendations expressed in this material are those of the authors and do not necessarily reflect the views of the National Science Foundation and National Research Foundation of Korea.

References

- [1] T.C.E. Ho, D. Surry, D. Morrish, G.A. Kopp, The UWO contribution to the NIST aerodynamic database for wind loads on low buildings: Part 1. Archiving format and basic aerodynamic data, Journal of Wind Engineering and Industrial Aerodynamics 93 (2005) 1–30. https://doi.org/10.1016/j.jweia.2004.07.006.
- [2] A. Hunt, Wind-tunnel measurements of surface pressures on cubic building models at several scales, Journal of Wind Engineering and Industrial Aerodynamics 10 (1982) 137–163. https://doi.org/10.1016/0167-6105(82)90061-7.
- [3] K.S. Kumar, T. Stathopoulos, Wind Loads on Low Building Roofs: A Stochastic Perspective, Journal of Structural Engineering 126 (2000) 944–956. https://doi.org/10.1061/(asce)0733-9445(2000)126:8(944).
- [4] Y. Ozmen, E. Baydar, J.P.A.J. van Beeck, Wind flow over the low-rise building models with gabled roofs having different pitch angles, Build Environ 95 (2016) 63–74. https://doi.org/10.1016/j.buildenv.2015.09.014.
- [5] Y. Tamura, H. Kikuchi, K. Hibi, Extreme wind pressure distributions on low-rise building models, Journal of Wind Engineering and Industrial Aerodynamics 89 (2001) 1635–1646. https://doi.org/10.1016/S0167-6105(01)00153-2.
- [6] M. Endo, B. Bienkiewicz, H.J. Ham, Wind-tunnel investigation of point pressure on TTU test building, Journal of Wind Engineering and Industrial Aerodynamics 94 (2006) 553–578.

- This file is the final accepted version of the manuscript published in https://doi.org/10.1016/j.jobe.2024.108651 https://doi.org/10.1016/j.jweia.2006.01.019.
- [7] P.L. Fernández-Cabán, F.J. Masters, Experiments in a Large Boundary Layer Wind Tunnel: Upstream Terrain Effects on Surface Pressures Acting on a Low-Rise Structure, Journal of Structural Engineering 146 (2020) 04720002. https://doi.org/10.1061/(asce)st.1943-541x.0002690.
- [8] American Society of Civil Engineers, Minimum Design Loads and Associated Criteria for Buildings and Other Structures, American Society of Civil Engineers, Reston, VA, 2017. https://doi.org/10.1061/9780784414248.
- [9] T.C.E. Ho, D. Surry, A.G. Davenport, Variability of low building wind loads due to surroundings, 1991.
- [10] H. Kiefer, E.J. Plate, Modelling of mean and fluctuating wind loads in built-up areas, Journal of Wind Engineering and Industrial Aerodynamics 74–76 (1998) 619–629. https://doi.org/10.1016/S0167-6105(98)00056-7.
- [11] J.D. Holmes, Wind pressures on tropical housing, Journal of Wind Engineering and Industrial Aerodynamics 53 (1994) 105–123. https://doi.org/10.1016/0167-6105(94)90021-3.
- [12] J.W. Zhang, Q.S. Li, Field measurements of wind pressures on a 600 m high skyscraper during a landfall typhoon and comparison with wind tunnel test, Journal of Wind Engineering and Industrial Aerodynamics 175 (2018) 391–407. https://doi.org/10.1016/j.jweia.2018.02.012.
- [13] A. Flaga, A. Kocoń, R. Kłaput, G. Bosak, The environmental effects of aerodynamic interference between two closely positioned irregular high buildings, Journal of Wind Engineering and Industrial Aerodynamics 180 (2018) 276–287. https://doi.org/10.1016/j.jweia.2018.07.024.
- [14] B. Chen, L. Shang, M. Qin, X. Chen, Q. Yang, Wind interference effects of high-rise building on low-rise building with flat roof, Journal of Wind Engineering and Industrial Aerodynamics 183 (2018) 88–113. https://doi.org/10.1016/j.jweia.2018.10.019.
- [15] B. Chen, W. Cheng, H. Ma, Q. Yang, Wind Interference Effects from One High-Rise Building and Similar Low-Rise Flat-Roof Buildings, Journal of Structural Engineering 147 (2021).

- This file is the final accepted version of the manuscript published in https://doi.org/10.1061/(asce)st.1943-541x.0003121.
- [16] G. Hu, L. Liu, D. Tao, J. Song, K.T. Tse, K.C.S. Kwok, Deep learning-based investigation of wind pressures on tall building under interference effects, Journal of Wind Engineering and Industrial Aerodynamics 201 (2020) 104138. https://doi.org/10.1016/j.jweia.2020.104138.
- [17] Z.N. Xie, M. Gu, Mean interference effects among tall buildings, Eng Struct 26 (2004) 1173–1183. https://doi.org/10.1016/j.engstruct.2004.03.007.
- [18] L.D. Sy, H. Yamada, H. Katsuchi, Interference effects of wind-over-top flow on high-rise buildings, Journal of Wind Engineering and Industrial Aerodynamics 187 (2019) 85–96. https://doi.org/10.1016/j.jweia.2019.02.001.
- [19] W. Kim, Y. Tamura, A. Yoshida, Interference effects on local peak pressures between two buildings, Journal of Wind Engineering and Industrial Aerodynamics 99 (2011) 584–600. https://doi.org/10.1016/j.jweia.2011.02.007.
- [20] X.F. Yu, Z.N. Xie, X. Wang, B. Cai, Interference effects between two high-rise buildings on wind-induced torsion, Journal of Wind Engineering and Industrial Aerodynamics 159 (2016) 123–133. https://doi.org/10.1016/j.jweia.2016.10.011.
- [21] X. Yu, Z. Xie, M. Gu, Interference effects between two tall buildings with different section sizes on wind-induced acceleration, Journal of Wind Engineering and Industrial Aerodynamics 182 (2018) 16–26. https://doi.org/10.1016/j.jweia.2018.09.012.
- [22] X. Du, H. Xu, W. Ma, C. Dai, Q. Liu, Experimental study on aerodynamic characteristics of two square cylinders at various incidence angles, Journal of Wind Engineering and Industrial Aerodynamics 191 (2019) 154–169. https://doi.org/10.1016/j.jweia.2019.05.019.
- [23] Q.S. Liang, J.Y. Fu, Z. Li, B.W. Yan, Z.R. Shu, Y.C. He, Bimodal distribution of wind pressure on windward facades of high-rise buildings induced by interference effects, Journal of Wind Engineering and Industrial Aerodynamics 200 (2020) 104156. https://doi.org/10.1016/j.jweia.2020.104156.

- This file is the final accepted version of the manuscript published in https://doi.org/10.1016/j.jobe.2024.108651
- [24] C.-H. Chang, R.N. Meroney, The effect of surroundings with different separation distances on surface pressures on low-rise buildings, Journal of Wind Engineering and Industrial Aerodynamics 91 (2003) 1039–1050. https://doi.org/10.1016/S0167-6105(03)00051-5.
- [25] Y.C. Kim, Y. Tamura, S. Yoon, Proximity effect on low-rise building surrounded by similar-sized buildings, Journal of Wind Engineering and Industrial Aerodynamics 146 (2015) 150–162. https://doi.org/10.1016/j.jweia.2015.08.011.
- [26] Y.C. Kim, A. Yoshida, Y. Tamura, Influence of Surrounding Buildings on Wind Loads Acting on Low-Rise Building, Journal of Structural Engineering 139 (2013) 275–283. https://doi.org/10.1061/(asce)st.1943-541x.0000625.
- [27] Y.C. Kim, A. Yoshida, Y. Tamura, Characteristics of surface wind pressures on low-rise building located among large group of surrounding buildings, Eng Struct 35 (2012) 18–28. https://doi.org/10.1016/j.eng-struct.2011.10.024.
- [28] S. Ahmad, K. Kumar, Interference effects on wind loads on low-rise hip roof buildings, Eng Struct 23 (2001) 1577–1589. https://doi.org/10.1016/S0141-0296(01)00057-8.
- [29] B. Chen, H. Cheng, H. Kong, X. Chen, Q. Yang, Interference effects on wind loads of gable-roof buildings with different roof slopes, Journal of Wind Engineering and Industrial Aerodynamics 189 (2019) 198–217. https://doi.org/10.1016/j.jweia.2019.03.033.
- [30] G. Li, S. Gan, Y. Li, L. Wang, Wind-induced interference effects on low-rise buildings with gable roof, Journal of Wind Engineering and Industrial Aerodynamics 170 (2017) 94–106. https://doi.org/10.1016/j.jweia.2017.07.009.
- [31] K. Wang, T. Stathopoulos, The impact of exposure on wind loading of low buildings, in: Proceedings of the Structures Congress and Exposition, American Society of Civil Engineers, 2006: p. 9. https://doi.org/10.1061/40889(201)9.
- [32] L.-S. An, N. Alinejad, S. Kim, S. Jung, Experimental study on wind characteristics and prediction of mean

- This file is the final accepted version of the manuscript published in https://doi.org/10.1016/j.jobe.2024.108651 wind profile over complex heterogeneous terrain, Build Environ 243 (2023) 110719. https://doi.org/10.1016/j.buildenv.2023.110719.
- [33] K. Wang, T. Stathopoulos, Exposure model for wind loading of buildings, Journal of Wind Engineering and Industrial Aerodynamics 95 (2007) 1511–1525. https://doi.org/10.1016/J.JWEIA.2007.02.016.
- [34] D.M. Deaves, Computations of wind flow over changes in surface roughness, Journal of Wind Engineering and Industrial Aerodynamics 7 (1981) 65–94. https://doi.org/10.1016/0167-6105(81)90068-4.
- [35] N.J. Cook, The Deaves and Harris ABL model applied to heterogeneous terrain, Journal of Wind Engineering and Industrial Aerodynamics 66 (1997) 197–214. https://doi.org/10.1016/S0167-6105(97)00034-2.
- [36] W. Tian, A. Ozbay, H. Hu, An experimental investigation on the aeromechanics and wake interferences of wind turbines sited over complex terrain, Journal of Wind Engineering and Industrial Aerodynamics 172 (2018) 379–394. https://doi.org/10.1016/j.jweia.2017.11.018.
- [37] S. Jung, F.J. Masters, Characterization of open and suburban boundary layer wind turbulence in 2008 Hurricane Ike, Wind and Structures, An International Journal 17 (2013) 135–162. https://doi.org/10.12989/was.2013.17.2.135.
- [38] R.W. Macdonald, R.F. Griffiths, D.J. Hall, An improved method for the estimation of surface roughness of obstacle arrays, Atmos Environ 32 (1998) 1857–1864. https://doi.org/10.1016/S1352-2310(97)00403-2.
- [39] N.J. Cook, Towards better estimation of extreme winds, Journal of Wind Engineering and Industrial Aerodynamics 9 (1982) 295–323. https://doi.org/10.1016/0167-6105(82)90021-6.
- [40] J. Lieblein, Efficient methods of extreme-value methodology, Gaithersburg, MD, 1974. https://doi.org/10.6028/NBS.IR.74-602.